J. Mol. Biol. (1997) **267**, 505–519

JMB

On the Conformation of the Anticodon Loops of Initiator and Elongator Methionine tRNAs

David C. Schweisguth[1] and Peter B. Moore[1,2]*

[1]*Department of Molecular Biophysics and Biochemistry and* [2]*Department of Chemistry Yale University, New Haven CT, USA*

Corresponding author

The solution conformations of analogues of initiator and elongator tRNA anticodon stem-loops have been compared by NMR. The data indicate that both have conformations closely similar to those reported for crystalline elongator tRNAs. The two loops differ in their dynamics, however: that of the elongator analogue is more flexible than its initiator counterpart. The anticodon stem-loops of initiator tRNAs are more likely to be distinguished from those of elongator tRNAs during initiation on the basis of their distinctive stem sequences, than they are by differences in the conformations of their anticodon loops.

Keywords: initiator; methionine; tRNA; NMR; structure

Introduction

Two kinds of methionine tRNA are found in the cytoplasms of all cells: an initiator methionine tRNA, $tRNA_f^{Met}$ in eubactera and $tRNA_i^{Met}$ in eukaryotes, and an elongator methionine tRNA, $tRNA_m^{Met}$. Even though the two forms of methionine tRNA have the same anticodon sequence, and are aminoacylated by the same methionyl-tRNA synthetase, they have completely different functions. Initiator tRNAs deliver the methionine that is the first amino acid in every nascent polypeptide to the translational apparatus. Elongator methionine tRNAs are the carriers for all internal methionines. Consistent with their functions, initiator tRNAs interact specifically with initiation factors and bind exclusively to the ribosomal P site, while elongator tRNAs form complexes only with EF-1α (eukaryotes) or EF-Tu (prokaryotes) and are inserted only into the ribosomal A site.

Many sequence elements distinguish initiator tRNAs from elongator tRNAs, but one such element is common to both eubacteria and eukaryotes: a run of three Gs at the end of the 5′ side of their anticodon stems, and a run of complementary Cs on the 3′ side (Dube *et al*., 1969). This ''G:C stack'' is also found in most archaeal (Kuchino *et al*., 1982) and organellar initiator tRNAs, and virtually every initiator tRNA that does not have three G·C pairs at that location has two instead (Sprinzl *et al*., 1996). G:C stacks are present in the anticodon stems of less than 1% of elongator tRNAs.

In principle, the G:C stack could facilitate initiator tRNA recognition by presenting a unique set of groups to the environment in the context of an otherwise unremarkable structure. Alternatively, it could adopt, or cause adjacent residues to adopt, an unusual conformation. There has long been data suggesting that the latter might be the case. The anticodon loops of initiator tRNAs from several species are less sensitive to the single strand-specific nuclease, S_1, than those of elongator tRNAs, which suggests that initiator anticodon loops may have more compact conformations than elongator anticodon loops (Wrede & Rich, 1979; Wrede *et al*., 1979).

Site-directed mutation experiments have demonstrated that the nuclease resistance of the anticodon loop of *Escherichia coli* $tRNA_f^{Met}$ depends on its G:C stack (Seong & RajBhandary, 1987). Furthermore, isolated anticodon stem-loops show the same S_1 resistance as intact tRNAs, even if they do not include the normal modified bases (Wrede & Rich, 1979; Hartz *et al*., 1990). Anticodon stem-loop analogues with their G:C stacks reversed (CCC:GGG) are not S_1-resistant, and several with initiator anticodon stems, but different anticodon loop sequences are S_1-sensitive, showing that S_1 resistance cannot be conferred on every anticodon loop by a G:C stack (Hartz *et al*., 1990).

Abbreviations used: CMCT, cyclohexyl-*N*′-[2-(*N*-methylmorpholino)ethyl]carbodiimide *p*-toluene sulphonate; DEPC, diethylpyrocarbonate; p.p.m., parts per million; COSY, correlated spectroscopy; HSQC, heteronuclear single quantum coherence; NOE, nuclear Overhauser effect; NOESY, NOE spectroscopy; TOCSY, total correlation spectroscopy; heteroTOCSY, heteronuclear TOCSY; r.m.s.d., root mean square difference.

0022–2836/97/130505–15 $25.00/0/mb960903

S_1 resistance correlates with initiator function. Mutant initiator tRNAs bind to the P site of the ribosome in proportion to their S_1 resistance, and the ability of anticodon stem-loop analogues to form initiation-like complexes in the presence of IF3 correlates with S_1 resistance (Seong & RajBhandary, 1987). Thus S_1 resistance seems to be related in some way to an initiator tRNA anticodon stem-loop identity element that IF3 recognizes. Only recently have RajBhandary and colleagues been able to generate a tRNA capable of functioning as an initiator that is not S_1-resistant (Mandal *et al.*, 1996).

The conformations of initiator and elongator tRNAs have been compared crystallographically, but to no avail. The quality of the electron density map obtained for yeast $tRNA_i^{Met}$ is so poor in its anticodon region that the authors declined to interpret it (Schevitz *et al.*, 1979; Basavappa & Sigler, 1991). Nevertheless, a specific proposal for the conformation of its anticodon loop has been offered recently by others (Dirheimer *et al.*, 1995). The anticodon loop is much better defined in the 3.5 Å structure published for *E. coli* $tRNA_f^{Met}$ (Woo *et al.*, 1980), but the result is still not definitive. Its highly conserved anticodon loop base U33, which corresponds to the U in the anticodon loop of yeast $tRNA^{Phe}$ from which the U-turn gets its name, is flipped out into the solvent. The significance of this observation is unclear, however, because its conformation is stabilized by interactions with a neighboring molecule.

Chemical probing data support neither of the proposals advanced for the conformation of initiator anticodon loops (Wakao *et al.*, 1989). U33 is unreactive to CMCT in $tRNA_f^{Met}$, which suggests that it is not exposed to solvent, contrary to the prediction of the model proposed for *E. coli* $tRNA_f^{Met}$ (Woo *et al.*, 1980). Furthermore, A38's N7 atom is unreactive to DEPC, which is inconsistent with the model for yeast initiator tRNA presented by Dirheimer *et al.* (1995). These data are, however, consistent with the known structure of elongator tRNAs.

We describe below the results of a spectroscopic comparison of two oligonucleotides, one an analogue of an initiator anticodon stem-loop and the other an analogue of a methionine elongator anticodon stem-loop. The data indicate that initiator anticodon loops have solution conformations similar to the anticodon loop conformation observed in elongator tRNAs (Hingerty *et al.*, 1978; Holbrook *et al.*, 1978; Westhof & Sundaralingam, 1986; Westhof *et al.*, 1988). The difference between the anticodon loops of initiator and elongator tRNAs in sensitivity to S_1 nuclease is explained by the greater flexibility of the latter. It is likely that during initiation, the G:C stacks in initiator tRNA anticodon stems are recognized directly.

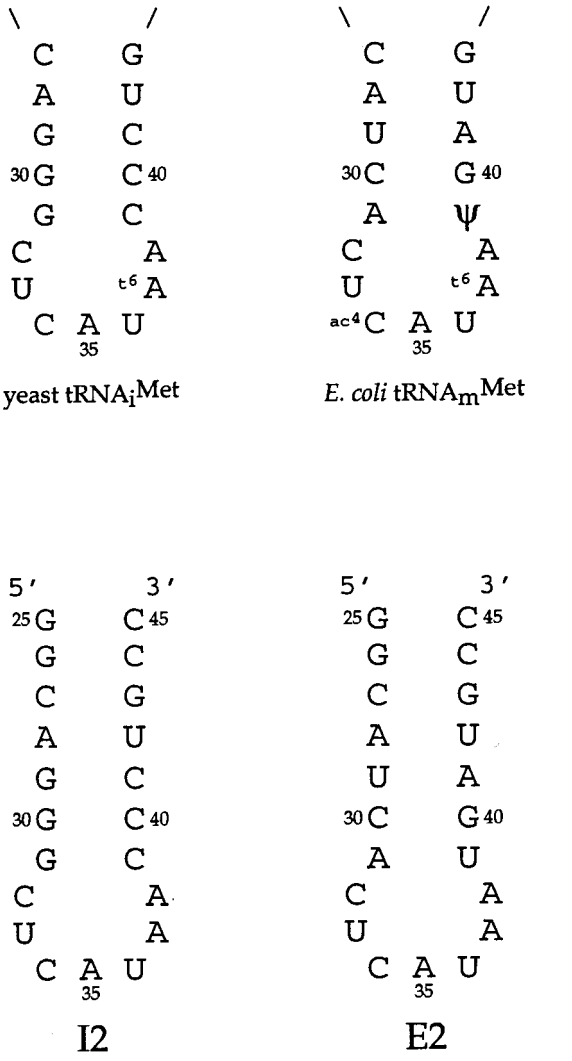

Figure 1. Initiator and elongator tRNA anticodon stem-loops in nature and in the versions studied in this work. Constructs are numbered to match the parent tRNAs.

Results

Figure 1 compares the sequences of the anticodon stem-loops of yeast initiator tRNA, *E. coli* methionine elongator tRNA, and the oligonucleotides designed to mimic them, I2 and E2. Two Gs were added to the 5′ ends of both oligonucleotides to make T7 transcription more efficient, and the opposing Cs were added to prevent aggregation (Szewczak *et al.*, 1990). Otherwise, except for the absence of modified bases, they are the same as their parental tRNAs, and their residues are numbered accordingly. The yeast and *E. coli* sequences were chosen because they differ only in the three base-pairs adjoining the anticodon loop.

Nuclease sensitivities of I2 and E2

Figure 2 shows the results of sequencing and S_1 nuclease cleavage experiments done on I2 and E2

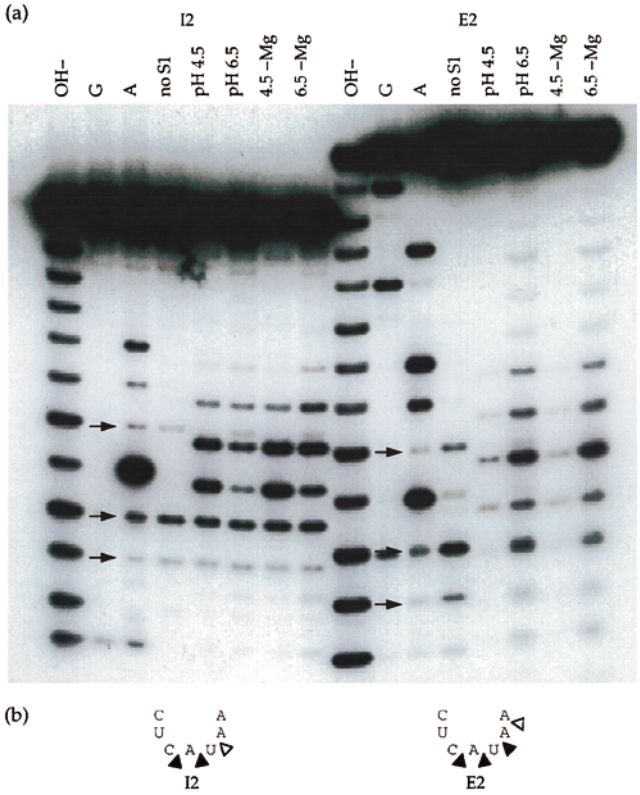

Figure 2. Sequencing and S_1 nuclease cleavage of I2 and E2. (a) Lanes 1 to 8, I2. Lanes 9 to 16, E2. Lanes 1 and 9, hydroxyl ladder. Lanes 2, 3, 10 and 11, T_1 (G-specific) and U_2 (A-specific) sequencing reactions. Lanes 4 to 8 and 12 to 16, S_1 cleavage reactions. Lanes 4, 5, 7, 12, 13 and 15, pH 4.5. Lanes 6, 8, 14 and 16, pH 6.5. Lanes 7, 8, 15 and 16, no Mg^{2+}. Lanes 4 and 12, no S_1. Arrows indicate non-enzymatic cleavage. (b) S_1 nuclease cleavage sites (lanes 5 and 13) displayed on the sequences of the loops of I2 and E2.

in buffers similar to those used for spectroscopy. Its interpretation is complicated by several factors. (1) On sequencing gels, S_1 fragments run almost one ''nucleotide'' slower than hydroxide, T_1 and U_2 fragments of the same length because cleavage of RNA by hydroxide ion and by T_1 and U_2 nucleases produce 3′ cyclic phosphates, but cleavage by S_1 nuclease produces 3′ hydroxyls. (2) Even in the absence of base or nucleases, I2 and E2 are cleaved to some extent by an agent we could not control, most strongly between C34 and A35 but also between U33 and C34 and between U36 and A37. (Similar cleavage has been seen in intact initiator tRNA (Wakao *et al.*, 1989).) Since the spontaneous cleavage products comigrate with hydroxide cleavage products, they can be distinguished from S_1 cleavage products. (3) When equal amounts of labelled I2 and E2 are cleaved and visualized under the same conditions, the S_1 cleavage products of E2 are fainter than those of I2 because E2 fragments are more susceptible to secondary cleavage than I2 fragments.

These problems notwithstanding, it is clear that I2 is cleaved by S_1 nuclease after C34 and A35, and less strongly after U36, while E2 is cleaved after C34, A35, U36 and less strongly after A37. Thus the strong cleavages observed here are the same as those reported earlier for tRNA anticodon loops (Wrede *et al.*, 1979; Wrede & Rich, 1979), except for the cleavage reported between U33 and C34, which is very weak here.

The cleavage patterns of both molecules are unaffected by magnesium (compare lanes 5 and 7). They are also unaffected by pH over the range from 4.5, which is the optimum for S_1 nuclease, to 6.5, at which pH Zn^{2+} is still soluble but the activity of S_1 is reduced (compare lanes 5, 7, 13 and 15 to 6, 8, 14 and 16). Fragments of E2 are less susceptible to secondary cleavage at high pH than they are at low pH, and cleavage can be seen continuously from U33/C34 to A37/A38. (The U33/C34 cleavage band is very close to a spontaneous cleavage band.) Although S_1 requires Zn^{2+}, which precipitates at alkaline pH, it has been reported that the patterns of cleavage of initiator and elongator tRNAs were maintained at pHs as high as 7.4 (Wrede & Rich, 1979), in agreement with our observations. The same results were obtained when these experiments were repeated in a buffer with twice this salt concentration, consistent with the earlier report that the S_1 resistance of initiator tRNAs is insensitive to ionic strength (Wrede & Rich, 1979).

The conclusion drawn from these observations is that I2 and E2 are reasonable model systems in which to compare the conformations of initiator and elongator tRNA anticodon loops, and that the buffer conditions chosen for their spectroscopic comparison are appropriate.

Initial characterization of I2 and E2

On non-denaturing polyacrylamide gels, both I2 and E2 have an electrophoretic mobility in NMR buffer that is less than that of a 17-nucleotide stem-loop, but greater than that of a 30-nucleotide stem-loop. This is true from 5°C to 30°C. In addition, optical melting experiments done in NMR buffer revealed that the melting profiles of both oligonucleotides are independent of concentration between 0.6 and 60 μM. Thus, under the conditions chosen for spectroscopic study, both molecules are monomeric stem-loops, not duplexes.

The melting temperatures predicted for I2 and E2 from their sequences are 99.5°C and 83.7°C, respectively (Zuker, 1989). The melting temperatures observed in NMR buffer were lower, 85°C and 72°C, respectively, which is not surprising because the ionic strength of NMR buffer is significantly less than 1 M, the condition in which the reference data were collected. Thus it would appear that there is no need to invoke loop interactions specific to I2 in order to account for the difference in stability between I2 and E2.

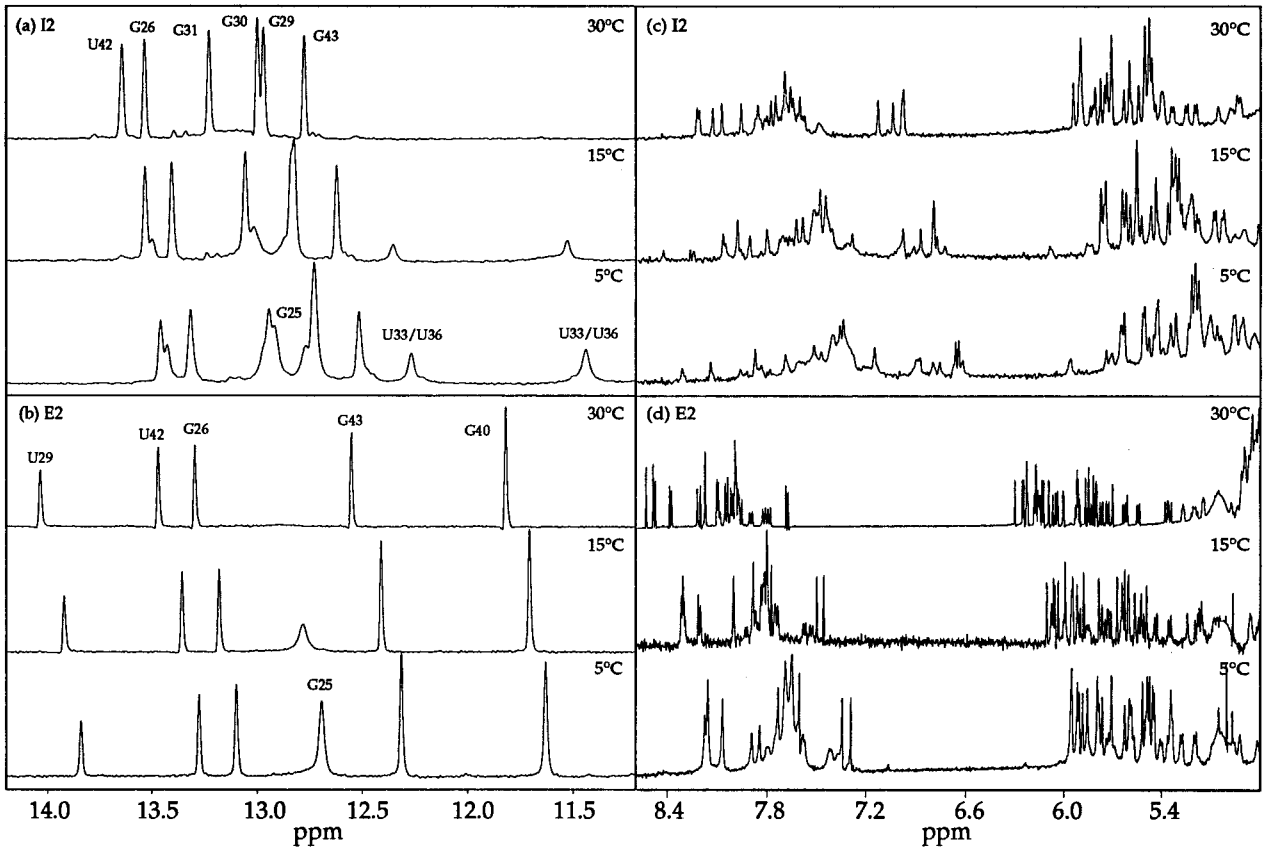

Figure 3. (a, b) One-dimensional imino spectra of (a) I2 and (b) E2 at 5, 15 and 30°C. All peaks represent GH1 or UH3 protons. (c, d) One-dimensional non-exchangeable proton spectra of (c) I2 and (d) E2 at 5, 15 and 30°C.

Figure 3 compares the effect of temperature on the proton spectra of I2 and E2. At 30°C, there are six imino proton resonances in the downfield spectrum of I2 (Figure 3(a)), which correspond to base-pairs G26·C44 through G31·C39 (see below). At 5°C, a resonance belonging to the imino proton of the terminal base-pair (G25H1) appears at 12.9 p.p.m., as do two new upfield resonances which, by elimination, must represent U33H3 and U36H3. The imino proton spectrum of E2 (Figure 3(b)) is less sensitive to temperature. The only resonance that materializes in its downfield spectrum at low temperatures is that of G25H1.

While it was tempting to conclude that the loop resonances observed in the downfield spectrum of I2 at 5°C indicate that initiator tRNAs have their unique anticodon loop conformation at all temperatures, further observations demonstrated that this is not the case. Unlike the resonance of G25H1, the resonances of U33 and U36 are clearly substoichiometric, and they appear in concert with a multitude of resonances that are even weaker. The thermal behaviour of the non-exchangeable proton spectrum of I2 is similarly complex (Figure 3(c)). As the temperature falls, new resonances appear, high temperature resonances disappear, and linewidths increase markedly. Nothing comparable happens with E2 (Figure 3(d)). Since there is no evidence that I2 aggregates at low temperature (see above), these data indicate that a second loop conformation emerges as the temperature falls, in which U33H3 and U36H3 are protected from exchange.

For technical reasons, it proved impossible to collect all the data that would have been necessary to characterize the low temperature conformation of I2. The fragmentary data obtained support the second-conformation hypothesis, however. At low temperature, the number of pyrimidine H5-H6 crosspeaks observed in COSY spectra is greater than the number of pyrimidines in I2, which is not the case at 30°C. Furthermore, it was clear that a second set of NOE crosspeaks, which represent the loop, increases in intensity as the temperature falls, and does so at the expense of loop crosspeaks apparent at high temperatures. At 5°C, the low temperature set is about two-thirds as strong as the high temperature set.

While it would be interesting to understand the low-temperature conformation of I2 better, it is not germane to this study. The difference in nuclease sensitivity that distinguishes initiator and elongator anticodon loops is fully apparent at 30°C, and initiator and elongator tRNAs are discriminated from each other *in vivo* at temperatures higher than that. Consequently, all the spectroscopy reported below was performed at 30°C.

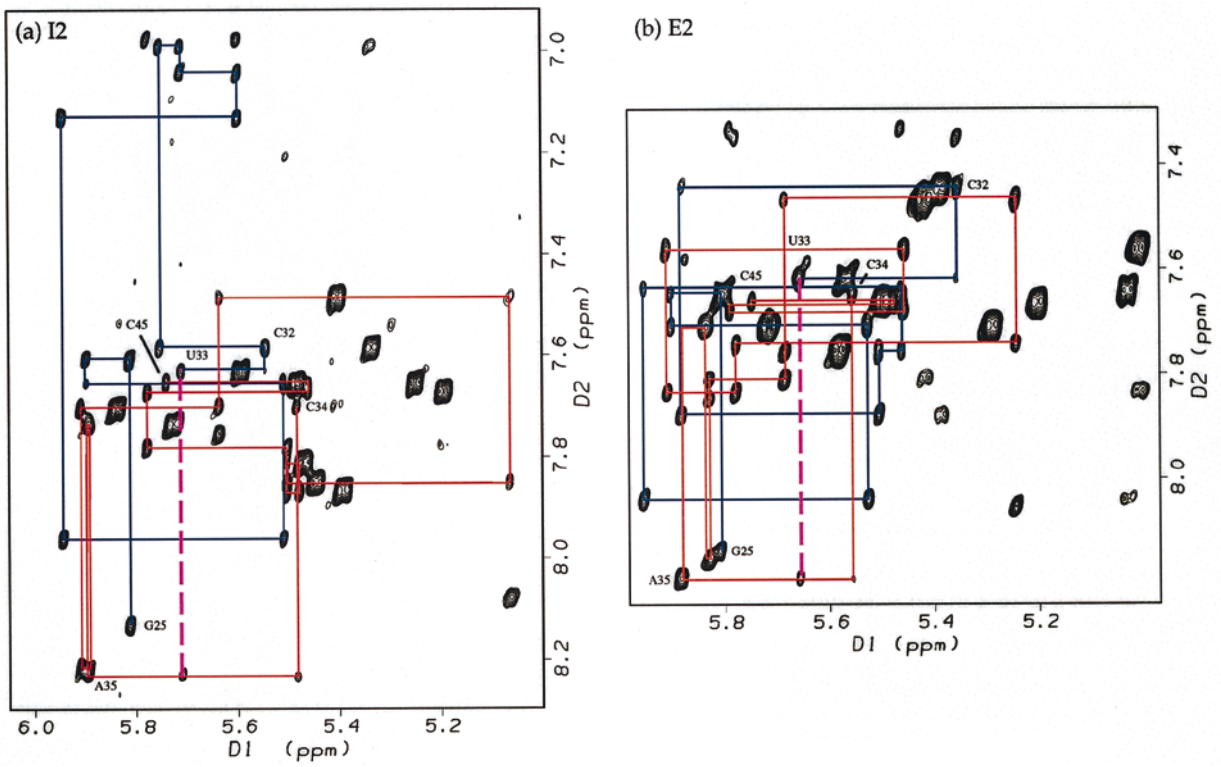

Figure 4. Anomeric-aromatic regions of 300 ms NOESY spectra of (a) I2 and (b) E2. Connectivities from G25 through U33 are in blue, connectivities from C34 to C45 are in red, and the U33H1′-A35H8 NOE is in purple.

Assignment of I2 resonances

The assignment of RNAs usually begins with an analysis of their imino proton spectra, and then proceeds to the sequential assignment of the resonances of anomeric and aromatic protons (Wüthrich, 1986; Moore, 1995). In this instance it proved easier to assign anomeric and aromatic resonances first, and then return to the imino proton resonances.

The aromatic-anomeric region of a 300 ms NOESY spectrum of I2 is shown in Figure 4. An *A*-form-like connectivity can be traced from G25H1′ to C45H6 that has a single break between U33H1′ and C34H6. Only one crosspeak is observed that is not *A*-like; it correlates U33H1′ and A35H8. The aromatic and anomeric assignments derived from this NOESY experiment were supported by two additional experiments: a COSY experiment, which identified pyrimidine H5-H6 crosspeaks, and a natural abundance ^{13}C-^{1}H HSQC experiment, which distinguished UH5s from CH5s and established the chemical identities of other proton resonances.

Imino proton resonances were assigned on the basis of the imino-aromatic and imino-anomeric crosspeaks observed in NOESY spectra collected in water (Wüthrich, 1986; Heus & Pardi, 1991). The assignments obtained indicated that the imino-imino crosspeaks observed link G26H1 to G43H1, U42H3 to G29H1, and G30H1 to G31H1.

Since six of the riboses in I2 have appreciable C2′-*endo* character, it was possible to identify their H2′ resonances from anomeric-ribose crosspeaks detected in COSY spectra (Figure 5(a)). The rest could be assigned from a NOESY spectrum collected at short mixing time because H2′ protons are closer to H1′ protons than any other, regardless of sugar pucker. At longer mixing times intranucleotide H1′-H4′ crosspeaks appear, so the resonances of most H4′ protons could be assigned from NOESY spectra as well.

Phosphorus resonances were assigned from a heteroTOCSY-NOESY spectrum. Correlations were observed relating every phosphorus (except those at termini) to two aromatic proton resonances, those of the bases on either side of the corresponding phosphate group, and crosspeaks were also observed correlating each phosphorus with the H1′ on its 5′ side and some with the H1′ on their 3′ sides (data not shown). Once the phosphorus spectrum was assigned, H3′ resonances could be identified using a ^{31}P-^{1}H COSY spectrum, which contained 20 strong, distinct crosspeaks, as expected. C45H3′ did not give a crosspeak in this spectrum because it is not adjacent to a phosphorus. It was assigned by its distinctive ^{13}C chemical shift (Varani & Tinoco, 1991).

Several experiments were used to assign the remaining 5′/5″ and 4′ protons. Many H5′/H5″ pairs could be correlated with one another in ^{13}C-^{1}H HSQC spectra by their shared carbon chemical shifts. A proton-proton TOCSY experiment executed with a mixing time of 200 ms transferred substantial magnetization from H1′ resonances to other sugar proton resonances, even in those parts of the molecule where riboses are rigidly C3′-*endo*

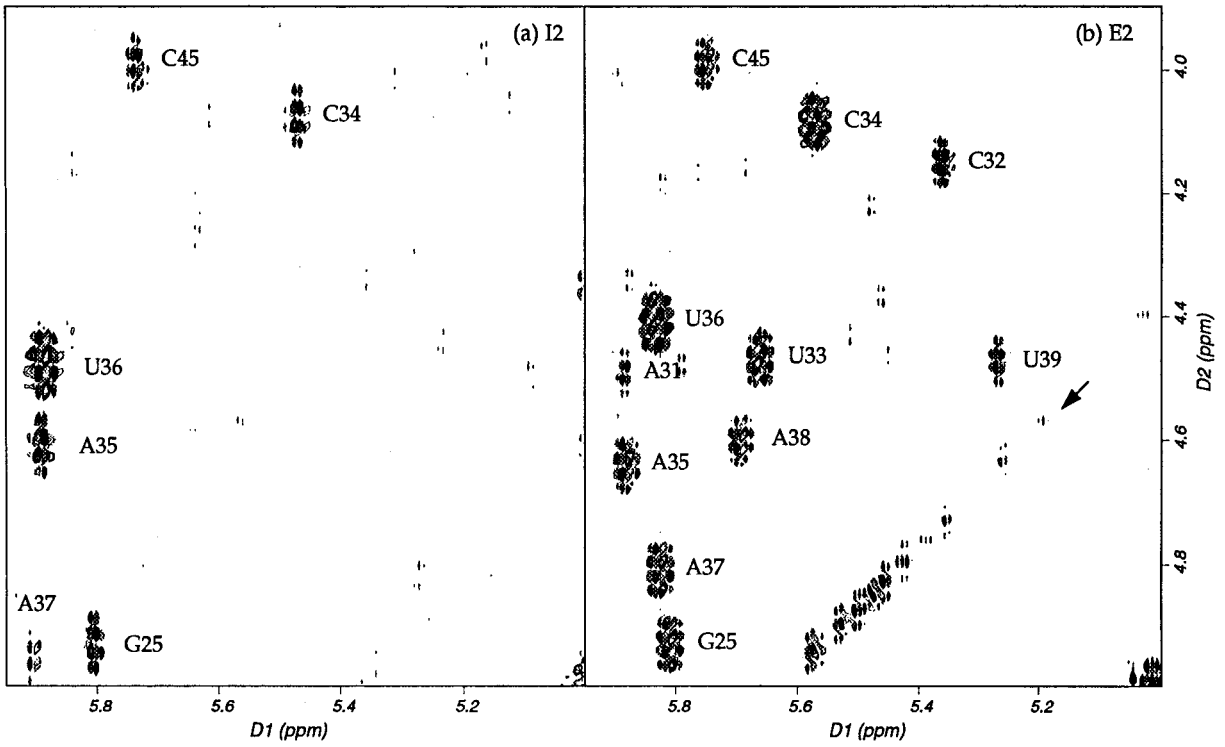

Figure 5. 1′-2′ regions of COSY spectra of (a) I2 and (b) E2. The chemical shift range on each axis includes all 1′ or 2′ protons in both molecules. Low-intensity crosspeaks arising from C2′-*endo* riboses are not labelled. The diagonal line indicated by the arrow is an artifact. The peaks at 5.0,5.0 are on the diagonal.

and 0.5 Hz $^{3}J_{H1'-H2'}$ couplings prevail. A heteroTOCSY spectrum correlated phosphorus resonances with the 5′/5″ and sometimes 4′ protons of the riboses on their 3′ sides. Finally, the aromatic-ribose regions of NOESY spectra contained intranucleotide H5′/5″-aromatic crosspeaks from which assignments could be gleaned. Stereospecific assignment of 5′ and 5″ protons was not attempted.

The proton and phosphorus assignments for I2 are summarized in Table 1. Virtually every assignment is supported by correlations observed in at least three different spectra or regions thereof. All protonated carbons had chemical shifts (not shown) which were consistent with their chemical types.

Qualitative features of I2

Several qualitative conclusions about the conformation of I2 can be drawn directly from its spectra. First, the pattern of NOEs in its stem indicates that it is *A*-form double helix, as anticipated. Second, the only region of the molecule where its conformation deviates significantly from that of an *A*-form helix is around U33, C34, and A35. Third, the absence of strong intranucleotide H1′-H6/H8 NOEs indicates that all its nucleotides are in the *anti* conformation. Fourth, the sugar pucker of its riboses are C3′-*endo* everywhere except in and immediately after the anticodon where they have values between those typical of *A* and *B*-form nucleic acids. Fifth, the chemical shifts of its phosphorus atoms indicate that its α and ζ angles are *A* form-like everywhere, except at C34, A35 and A37.

Constraints used for the calculation of the structure of I2

Table 2 summarizes the constraints on which structural computations were based. Since it was clear that the stem of I2 is *A*-form helix, and since that part of the molecule is uninteresting conformationally, the experimental data obtained from that part of the molecule was ignored, and it was artificially constrained to adopt ideal *A*-form conformation (see Materials and Methods).

Experimental data were considered in detail only for the seven loop nucleotides. The data available consisted of 128 distance constraints, 71 of them intraresidue and 57 of them interresidue, obtained from NOE spectra. All loop χ angles were constrained to *anti* values. U36's ribose was determined to be only 23% C3′-*endo* (Table 3) and was constrained to be C2′-*endo*. The riboses of C34, A35 and A37 had around 50% C3′-*endo* character and were left unconstrained. All other riboses were constrained to be C3′-*endo*.

Since the phosphates of C32, U33, U36 and A38 had chemical shifts similar to those found in *A*-form RNA, their α and ζ angles were constrained to *A*-form values (Gorenstein, 1984) (Table 4). The absence of intense crosspeaks between phosphorus and 5′ or 5″ protons in the heteroTOCSY spectra indicated that all β dihedral angles are *trans*

Table 1. (A) I2 and (B) E2 proton and phosphorus chemical shifts

(A) *I2*

	H1/H3	NH1	NH2	H6/H8	H2/H5	H1′	H2′	H3′	H4′	H5′/′′	H5′/′′	P
G25	NO	NO	NO	8.13	NA	5.81	4.93	4.71	4.57	4.26	4.41	NO
G26	13.25	NO	NO	7.60	NA	5.90	4.56	4.56		4.27	4.51	−3.68
C27	NA	6.79	8.41	7.66	5.25	5.51	4.55	4.54	4.45	4.14		−4.26
A28	NA	NO	NO	7.96	6.98	5.94	4.66	4.68	4.50	4.15		−3.77
G29	12.69	NO	NO	7.13	NA	5.60	4.54	4.43		4.06		−3.91
G30	12.73	NO	NO	7.04	NA	5.71	4.60	4.39		4.03		−3.82
G31	12.95	NO	NO	6.99	NA	5.75	4.59	4.38	4.41	4.03	4.27	−3.78
C32	NA	NO	NO	7.59	5.33	5.55	4.31	4.42	4.37	4.09		−4.40
U33	NO	NA	NA	7.63	5.59	5.71	4.73	4.55	4.35	4.27	4.45	−3.71
C34	NA	NO	NO	7.70	5.83	5.48	4.07	4.36	4.19	4.00	4.02	−2.30
A35	NA	NO	NO	8.23	7.72	5.90	4.62	4.98	4.36	4.04	4.18	−3.35
U36	NO	NA	NA	7.74	5.73	5.89	4.48	4.71	4.51	4.20	4.29	−4.14
A37	NA	NO	NO	8.21	7.75	5.91	4.95	4.60	4.44	4.26		−3.07
A38	NA	NO	NO	7.70	8.08	5.64	4.14	4.44	4.53	4.20		−3.98
C39	NA	6.96	8.58	7.49	5.40	5.06	4.23	4.39		4.09	4.70	−4.60
C40	NA	6.91	8.46	7.85	5.44	5.50	4.36	4.52	4.40	4.06		−4.52
C41	NA	6.85	8.34	7.81	5.47	5.48	4.38	4.50	4.41	4.15	4.53	−4.33
U42	13.36	NA	NA	7.87	5.39	5.50	4.62	4.60	4.45	4.11		−4.28
G43	12.50	NO	NO	7.78	NA	5.78	4.48	4.59	4.62	4.13	4.54	−4.10
C44	NA	6.81	8.51	7.67	5.19	5.46	4.21	4.43	4.38	4.04		−4.52
C45	NA	NO	NO	7.66	5.48	5.74	3.99	4.16	4.45			−4.22

(B) *E2*

	H1/H3	NH1	NH2	H6/H8	H2/H5	H1′	H2′	H3′	H4′	H5′/′′	H5′/′′	P
G25	NO	NO	NO	8.14	NA	5.81	4.93	4.73	4.58	4.27	4.41	NO
G26	13.30	NO	NO	7.65	NA	5.91	4.56	4.60	4.54	4.28	4.52	−3.70
C27	NA	6.83	8.48	7.71	5.29	5.53	4.58	4.57	4.46	4.14		−4.27
A28	NA	NO	NO	8.04	7.33	5.96	4.51	4.64	4.69	4.05	4.16	−3.91
U29	14.04	NA	NA	7.64	5.03	5.46	4.37	4.43	4.42	4.12		−4.51
C30	NA	6.81	8.22	7.76	5.58	5.51	4.43	4.50	4.38			−4.14
A31	NA	NO	NO	7.88	7.35	5.88	4.50	4.58	4.44	4.12		−3.97
C32	NA	NO	NO	7.45	5.39	5.36	4.15	4.35	4.32	4.05		−4.17
U33	NO	NA	NA	7.62	5.57	5.66	4.49	4.50	4.27	4.03		−3.97
C34	NA	NO	NO	7.65	5.81	5.56	4.08	4.37	4.14	3.96	4.10	−2.99
A35	NA	NO	NO	8.20	7.85	5.89	4.65	4.88	4.36	4.03	4.17	−3.57
U36	NO	NA	NA	7.71	5.72	5.84	4.41	4.65	4.45	4.15	4.25	−4.09
A37	NA	NO	NO	8.15	7.76	5.83	4.81	4.65	4.52	4.22	4.36	−3.36
A38	NA	NO	NO	7.81	8.06	5.69	4.60	4.48	4.52	4.19	4.43	−3.83
U39	NO	NA	NA	7.47	5.42	5.24	4.47	4.51	4.42	4.10		−4.18
G40	11.82	NO	NO	7.75	NA	5.78	4.64	4.65	4.50	4.18		−3.87
A41	NA	NO	NO	7.84	7.65	5.91	4.46	4.62	4.50	4.14	4.39	−4.10
U42	13.47	NA	NA	7.56	5.01	5.46	4.47	4.50	4.40	4.06		−4.38
G43	12.55	NO	NO	7.68	NA	5.79	4.48	4.56	4.14	4.12	4.17	−4.04
C44	NA	6.81	8.54	7.67	5.20	5.48	4.22	4.43	4.39	4.04		−4.52
C45	NA	NO	NO	7.66	5.50	5.75	3.99	4.16	4.47	4.01	4.16	−4.22

NA, Not Applicable (that nucleotide does not have such a spin). NO, Not Observed. H5′s and H5′′s are not stereospecifically assigned.

(Varani & Tinoco, 1991). Phosphorus-H4′ cross-peaks were observed for all loop nucleotides excepting A35 and U36, confirming that β is *trans* for these nucleotides, and establishing that γ is *trans* also (Varani & Tinoco, 1991). ε was constrained not to be *gauche*$^+$ for all loop nucleotides (Varani & Tinoco, 1991) (see Materials and Methods).

Structural computations

Of the 30 structures computed for I2 (see Materials and Methods), 12 violated no constraints and had low total energy. The rate of convergence was sensitive to the number, accuracy and precision of the constraints used, and to the temperature and duration of the simulated annealing. It varied between 10% and 80% as the protocols and input data were developed.

The dihedral angles of all the converged structures of I2 were similar except for the α, β and γ dihedral angles of A35, which had one set of values in nine structures and another in the other three. Table 5 lists their average values and standard deviations, which were calculated using all 12 structures, except for A35's α, β and γ dihedral angles, which were calculated separately over the sets of nine and three structures. The coordinates of the set of nine structures were averaged and the result-

Table 2. Experimental observations and the resulting constraints on the structure of I2

Observation	Constraint	No.
Stem		1736
Non-exchanging imino protons	Distances between Watson-Crick hydrogen-bonding partners	20
	Planarity of paired bases	7
A-form helical RNA	*A*-form distances	1560
	A-form dihedral angles	149
Loop		182
Nuclear Overhauser effect	Proton-proton distances	
	Short (2.4 ± 0.6 Å)	27
	Medium (3 ± 1 Å)	33
	Long (4 ± 1 Å)	68
	Total	128
	χ Glycosidic dihedral angles	7
H1′-H2′ coupling constants	ν_0-ν_4 ribose dihedral angles	20
^{31}P chemical shifts in *A*-form range	α and ζ backbone dihedral angles	8
^{31}P-^{1}H coupling constants	β and γ backbone dihedral angles	12
Steric exclusion	ε Backbone dihedral angle	7

ing structure energy-minimized to produce the final structure.

All 12 converged structures are shown with their loops superimposed on that of the average structure in Figure 6. The r.m.s.d. between individual loops and the average loop (residues 32 to 38) was 0.6 Å. Individual loop r.m.s.d.s ranged from 0.3 Å to 0.9 Å.

It is worth noting that the parameter and topology files used here lack an improper angle term to preserve the chirality of the phosphate oxygens O1P and O2P. Consequently their chirality sometimes changed during simulated annealing. This had no effect on structure calculations, since these atoms were not involved in any experimental constraints, but it did inflate root mean squared deviations when structures were compared. Since this problem was discovered after calculations were complete, calculated structures were ''repaired'' after the fact by manual editing, and this repair reduced r.m.s.d.s by about 0.3 Å. We suspect that some of the estimates of nucleic acid r.m.s.d.s in the literature suffer from this defect.

Description of the structure of the loop of I2

Figure 7 shows the loop nucleotides of the average structure. On the 5′ side of the loop, C32 stacks on G31 and U33 stacks to some degree on C32. There is a sharp turn between U33 and C34, almost entirely because C34's α dihedral angle is *trans* rather than the normal *gauche*$^-$. On the 3′ side, C34 through A38 stack on C39. The C2′-*endo* ribose ring of U36 is responsible for a kink between U36 and A37. C34's ribose is also relatively extended, while those of A35 and A37 are close to C3′-*endo*.

The sharp turn in this structure is qualitatively similar to the ''U-turns'' first identified in the anticodon loops of crystalline elongator tRNAs, as the superposition of the I2 loop on the anticodon loop of tRNA^{Phe} (Hingerty *et al*., 1978) shown in Figure 8 makes clear. The r.m.s.d. between non-hydrogen backbone atoms in the two loops is 1.2 Å. (By way of comparison, the r.m.s.d. between the same atoms in two independently determined structures of tRNA^{Phe} (Hingerty *et al*., 1978; Holbrook *et al*., 1978) is 0.8 Å.) While this is the best quantitative comparison that can be made between I2 and tRNA^{Phe} because of their different sequences, it un-

Table 3. H1′-H2′ coupling constants and fractional C3′-*endo* characters for (A) I2 and (B) E2

Residue	A. *I2* $^{3}J_{H1'-H2'}$	$f_{C3'\text{-}endo}$	Residue	B. *E2* $^{3}J_{H1'-H2'}$	$f_{C3'\text{-}endo}$
G25	3.60	62.7	G25	3.60	62.7
			A31	2.45	79.4
			C32	2.55	77.9
			U33	3.15	69.2
C34	4.90	43.8	C34	3.70	61.3
A35	4.50	49.7	A35	4.40	51.1
U36	6.30	23.6	U36	5.25	38.8
A37	3.80	59.8	A37	3.20	68.5
			A38	2.40	80.1
			C39	2.15	83.7
C45	4.20	54.0	C45	2.75	75.0

Table 4. Structural constraints on backbone dihedral angles in the loop if I2

Residue	α	β	γ	ε	z
C32	A	A	A	Not g^+	A
U33	A	A	A	Not g^+	None
C34	None	A	A	Not g^+	None
A35	None	A	None	Not g^+	A
U36	A	A	None	Not g^+	None
A37	None	A	A	Not g^+	A
A38	A	A	A	Not g^+	A

A means that the angle was constrained to the *A*-form value ±30°, not g^+ that the angle was constrained to not be *gauche*$^+$, and none that the angle was not constrained.

derstates the difference between the orientations of their bases. Although the bases of C32, U33, A37 and A38 superimpose well on the equivalent bases in $tRNA^{Phe}$, the bases in the anticodon of the NMR structure are tilted about 40° towards the tip of the loop. This appears to be a consequence of the C2′-*endo* conformation of U36's ribose.

The loop of I2 may include two of the three hydrogen bonds found in crystal structures of U-turns (Jack *et al*., 1976): U33N3 is 2.9 Å from U36O2P and U33O2′ is 2.9 Å from A35N7, just as in $tRNA^{Phe}$. However, A35N6 is further from U33O2′ than expected, 4.3 Å instead of 3.1 Å. The non-Watson-Crick base-pairing identified at the base of $tRNA^{Phe}$'s anticodon loop may also be present: A38N6 is 3.5 Å from C32O2, which is closer than reported in $tRNA^{Phe}$ (4.2 Å).

Assignment of E2

The spectra of E2 were assigned exactly the same way as were those of I2. It was easy to do because E2 proton resonances have essentially the same chemical shifts as corresponding I2 proton resonances, except where their sequences differ (compare Tables 1a and 1b). The chemical shifts of protonated carbons were unremarkable and are not shown. As is evident from Table 1b, it was possible to assign the spectra of E2 more completely than those of I2 due to the superior quality of the sample used, the wider chemical shift dispersion in its stem, and its larger H1′-H2′ couplings, which made proton-proton TOCSY experiments more revealing. The $^3J_{H1'\text{-}H2'}$ data obtained are given in Table 3.

Qualitative features of E2

I2 and E2 are very similar. They are both stem-loops. As comparison of Figure 4(a) and (b) shows, the loop NOEs of the two molecules are identical, the non-sequential U33H1′-A35H8 NOE in both molecules being diagnostic of a U-turn. Phosphorus atoms with unusual chemical shifts are found at the same positions. Moreover, in the loop, where their sequences are identical, the chemical shifts are virtually identical. The conformations of I2 and E2 must be basically the same.

There are some differences, however. First, in E2, U39H3, which ought to make a hydrogen bond with A31N1 in the last base-pair of the stem, does not have an observable resonance at any temperature. The closing base-pair of the E2 loop must be less stable than that of I2. Second, while in the I2 loop H1′-H2′ couplings were measurable only in the riboses of C34 through A37, all of the loop riboses in E2 have appreciable C2′-*endo* character, as do the riboses of what on paper should be the last

Table 5. Average values of dihedral angles in the calculated structures of I2, ± standard deviations

	α	β	γ	ε	ζ	χ
C32	−67 ± 3	−165 ± 2	44 ± 2	−122 ± 8	−84 ± 8	−162 ± 2
U33	−43 ± 3	164 ± 5	39 ± 4	−156 ± 9	−52 ± 9	−163 ± 4
C34	121 ± 19	163 ± 7	70 ± 6	−110 ± 11	−83 ± 11	−130 ± 6
A35	−104 ± 14	158 ± 5	56 ± 11	−169 ± 3	−67 ± 3	−126 ± 3
	86 ± 2	−151 ± 0	175 ± 1			
U36	−66 ± 5	171 ± 2	69 ± 2	−98 ± 1	−94 ± 9	−127 ± 0
A37	−90 ± 19	153 ± 1	53 ± 12	−159 ± 0	−70 ± 2	−149 ± 2
A38	−64 ± 1	149 ± 0	83 ± 0	−117 ± 0	−67 ± 0	174 ± 2

	ν_0	ν_1	ν_2	ν_3	ν_4
C32	14 ± 1	−29 ± 1	33 ± 0	−25 ± 0	7 ± 1
U33	−1 ± 3	−19 ± 2	32 ± 1	−34 ± 1	22 ± 2
C34	−14 ± 4	21 ± 16	−20 ± 21	12 ± 20	0 ± 10
A35	−2 ± 5	−20 ± 3	34 ± 0	−36 ± 3	24 ± 5
U36	−29 ± 1	23 ± 2	−10 ± 2	−6 ± 2	22 ± 2
A37	12 ± 0	−34 ± 0	42 ± 0	−36 ± 0	14 ± 1
A38	4 ± 2	−27 ± 1	39 ± 0	−37 ± 1	20 ± 2

A35's α, β and γ are calculated over the sets of nine and three structures in which they each take on two distinct values.

Figure 6. The 12 converged structures of I2, in grey, superimposed on the average structure, in black. Superposition considered only the loop (nucleotides 32 to 38) to emphasize similarity in loop structure.

base-pair in the stem, U39:A31 (Figure 5(b)). E2's loop must be significantly more flexible than that of I2.

Additional insight into this difference in flexibility may be obtained by comparing the temperature dependence of the ^{31}P spectrum of E2 with that of I2 (Figure 9). The phosphorus atoms responsible for the downfield-shifted resonances in both molecules are the same (compare Tables 1 and 6), but at 30°C, they are shifted downfield much more strongly in I2 than in E2. The difference diminishes as the temperature drops, which suggests that the loop of E2 becomes less flexible, and converges on the conformation characteristic of I2. Incidentally, the fact that the pattern of downfield-shifted peaks in the ^{31}P spectrum of I2 at 5°C is not much different from what it is at 30°C

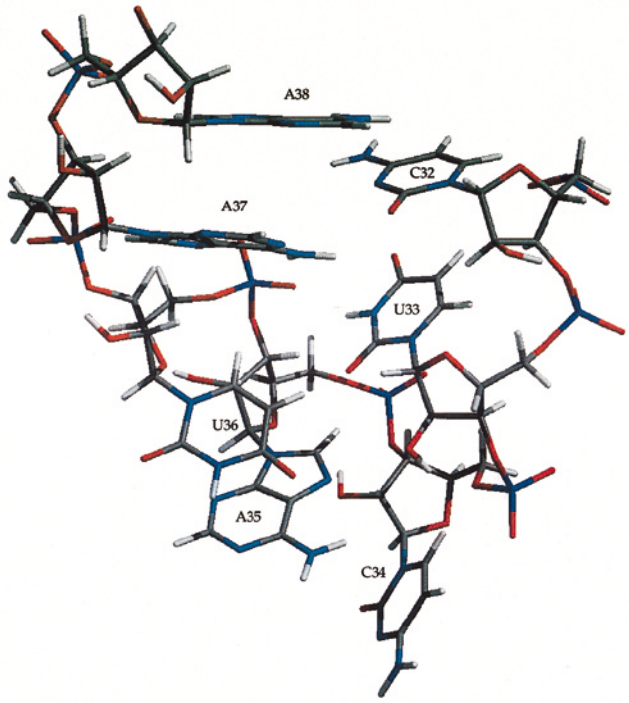

Figure 7. The loop of I2.

suggests that the low temperature conformer of I2 is not radically different from the one discussed here.

Discussion

There are many reasons for believing that the stem-loops studied here accurately model the anticodon arms of the tRNAs of interest. First, oligonucleotide stem-loops similar to I2 form initiation complexes properly (Hartz *et al.*, 1990). Second, I2 and E2 reproduce the S_1 nuclease cleavage patterns characteristic of initiator and elongator anticodon loops. Third, since anticodon stem-loops do not interact with the rest of their tRNAs, there is no reason to think that their removal from that context would alter their conformations. Fourth, since the anticodon loops of initiator tRNAs are less modified than other tRNAs, and the modifications they contain are not conserved, it is unlikely that the absence of modified bases from these oligonucleotides qualitatively affects their conformations.

Even though Mg^{2+} binds to the anticodon loop of $tRNA^{Phe}$ and stabilizes its conformation (Salemink *et al.*, 1981; Labuda & Porschke, 1982; Striker *et al.*, 1989), its omission from the buffer used here is unlikely to be significant. The ^{31}P spectrum of $tRNA_f^{Met}$ is almost unaffected by the removal of magnesium (Gorenstein & Goldfield, 1982); a single peak attributed to the anticodon loop of $tRNA_f^{Met}$ moves upfield a little in the absence of magnesium, but still retains the downfield shift indicative of a conformation other than *gauche*$^-$/

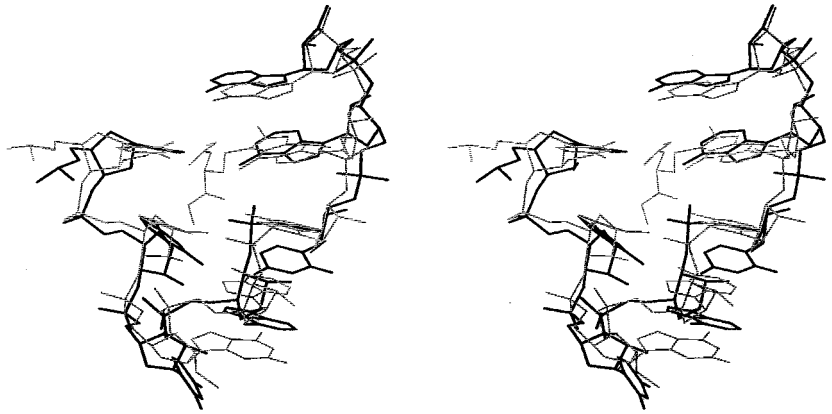

Figure 8. Superposition of the loop of I2 (black) on the anticodon loop of $tRNA^{Phe}$ (grey).

gauche$^-$. Furthermore, the solution structure of the $tRNA^{Phe}$ anticodon domain is the same in the absence of Mg^{2+} as it is in crystals of $tRNA^{Phe}$ that contain Mg^{2+} (Clore *et al.*, 1984). Finally, the S_1 cleavage patterns of $tRNA_f^{Met}$ (Wrede & Rich, 1979) and I2 (present work) are the same in the presence and absence of magnesium.

The conformation obtained for the loop of I2 is distinctly different from that of the anticodon loop observed in crystalline $tRNA_f^{Met}$ (Woo *et al.*, 1980) and from that proposed for the anticodon loop of yeast $tRNA_i^{Met}$ (Dirheimer *et al.*, 1995). What it does resemble is that of the anticodon loop of crystalline $tRNA^{Phe}$. The close similarity of the loop chemical shifts and NOE connectivities of I2 with those of E2 reinforces this conclusion. There is no major difference between the time-averaged anticodon loop conformations of initiator and elongator tRNAs. The significance of the minor differences detected between anticodon loops in solution and anticodon loops in tRNA crystals remains to be determined.

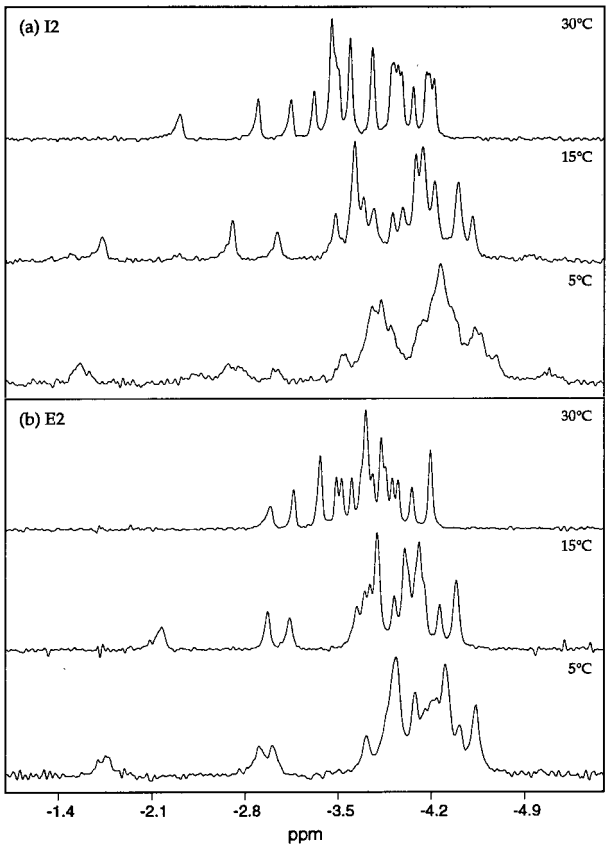

Figure 9. One-dimensional proton-decoupled phosphorus spectra of (a) I2 and (b) E2 at 5, 15 and 30°C.

The most distinctive feature of I2's anticodon loop is its U-turn. Turns like it are common in RNAs. The TψC loops in tRNAs contain a U-turn (Jack *et al.*, 1976), as does the hexaloop from the L11 binding site in 23 S rRNA (Huang *et al.*, 1996; Fountain *et al.*, 1996). A *bona fide* U-turn also occurs at the active site of the hammerhead ribozyme (Pley *et al.*, 1994; Scott *et al.*, 1995), and an octaloop from the T4 gp43 mRNA (Mirmira & Tinoco, 1996a) and a tetraloop mutant of it (Mirmira & Tinoco, 1996b) both have similar structures.

U-turns have a distinctive NMR "fingerprint". The anomeric proton of the residue n, where the turn begins, the U, gives an NOE to its own aromatic proton and to the aromatic proton of base $(n + 2)$, but not the normal, sequential NOE to that of its immediate neighbor, base $(n + 1)$. Also, the 2′ proton of base n gives NOEs to the aromatic protons of both base $(n + 1)$ and base $(n + 2)$. In addition, the phosphorus of the phosphate between residue n and residue $(n + 1)$ has a strong, downfield chemical shift, which reflects the fact that its α dihedral angle is *trans*. Turns based on *trans* α angles are called π turns (Saenger, 1983). U-turns are π turns, but not all π turns are U-turns.

The most obvious difference between I2 and E2 is the dynamics of their loop structures. The structure of I2 is more rigid, and its non-*A*-like properties are concentrated in its U-turn nucleotides and the C2′-*endo* ribose of U36. None of the loop nucleotides in E2 deviate from *A*-form conformation as radically as some of I2s, but the deviations are more widespread, consistent with its

sampling a wider range of conformations. Because the difference between I2 and E2 is primarily dynamic, no effort was made to model the average structure of E2.

It is not unreasonable that the anticodon loop of E2 is more flexible than that of I2. The A·U that closes its loop should stack less well on the underlying C·G pair (−1.8 kcal/mol) than should the loop-closing G·C of I2 on its underlying G·C (−2.9 kcal/mol) (Freier *et al.*, 1986). Furthermore, A·Us are weaker than G·Cs, and the C32-A38 mismatch may also stack differently on the loop-closing G·C and A·U pairs. These effects may account for the difference in loop flexibility, and elongator anticodon loops may be more sensitive to S_1 nuclease than those of initiators simply because of that difference in flexibility.

The loop of E2 switches between the conformations available to it so fast that its chemical shifts, scalar couplings and NOEs observed are averaged over an ensemble of conformational states. Thus its flexibility is not at all like that reported for a DNA analogue of the $tRNA^{Phe}$ anticodon loop, which exists in two different conformations, depending on Mg^{2+} concentration (Guenther *et al.*, 1992).

It is not certain at this point whether the flexibility of elongator tRNA anticodon loops is functionally significant, but the behaviour of methionine tRNA synthetase suggests that it is not. MetRS recognizes the sequence of the anticodon loop, but it does not discriminate between $tRNA_f^{Met}$ and $tRNA_m^{Met}$. The K_ds for binding of *E. coli* MetRS to *E. coli* $tRNA_f^{Met}$ and $tRNA_m^{Met}$ are 1.5 and 1.3 μM, respectively (Meinnel *et al.*, 1993), consistent with the finding that the structures of their anticodon loops are the same. Structure-based alignment indicates that MetRS is similar to glutaminyl-tRNA synthetase (GlnRS), which suggests that it binds tRNA in the same way (Perona *et al.*, 1991). GlnRS disrupts the anticodon loop of its substrate tRNA on binding (Rould *et al.*, 1989). The similarity of the K_ds with which MetRS binds initiator and elongator tRNAs thus suggests that the stabilities of the two anticodon loops are similar. If so, it is hard to see how initiator tRNAs can be discriminated from elongator tRNAs on that basis. It seems likely that the G·C stack in initiator tRNAs is the element that is recognized, not the structure of the adjacent anticodon loop, a proposal completely consistent with the recent finding that tRNAs can be generated that are competent to initiate but lack the insensitivity to S_1 nuclease characteristic of normal initiator tRNAs (Mandal *et al.*, 1996).

Materials and Methods

Oligonucleotides

Oligonucleotides were transcribed from chemically synthesized DNA templates using T7 RNA polymerase (Beckett & Uhlenbeck, 1984; Milligan *et al.*, 1987). Templates were double-stranded in their promoter regions and single-stranded elsewhere. Transcription products were purified by electrophoresis on denaturing gels, and recovered by electroelution.

S_1 nuclease cleavage

RNAs were 5′-end-labelled with ^{32}P, and were sequenced enzymatically (Maniatis *et al.*, 1982). The buffer for S_1 cleavage was 12.5 mM NaOAc, 25 mM KCl, 2.5 mM $MgCl_2$, 0.5 mM $ZnCl_2$ (pH 4.5) (Hartz *et al.*, 1990). For experiments run at pH 6.5 and 7.5, NaOAc was replaced with Na cacodylate. For experiments run without Zn^{2+}, $ZnCl_2$ was omitted and the $MgCl_2$ concentration raised to 10 mM. S_1 reactions were done at 5 μl scale. A typical reaction mixture included 1 μg of tRNA and labelled oligonucleotide, and one unit of nuclease (Sigma). They were incubated for 5 to 60 minutes at 37°C, and the products analysed on sequencing gels.

Non-denaturing gel electrophoresis

0.5 or 1 μl of RNA solution was removed directly from an NMR sample, and analysed on a 20% (w/v) polyacrylamide gel in NMR buffer (see below). The gel buffer was recirculated with a peristaltic pump to maintain a constant ionic composition. RNA was visualized with methylene blue.

UV melts

Aliquots of RNA were dialysed extensively against NMR buffer (see below), diluted to concentrations of 0.1, 0.3, 1, 3 and 10 OD, degassed under vacuum, and placed in stoppered quartz cuvettes with path lengths of 1 cm (0.1, 0.3 and 1 OD samples) or 0.1 cm (3 and 10 OD samples). Melting was done in a Varian Cary 1 UV-visible double-beam spectrophotometer. Five samples, one at each concentration, were melted simultaneously. Cuvettes filled with degassed buffer were used as references. The temperature was raised from 5 to 95°C at 0.5°C per minute and the absorbance at 260 nm of each sample recorded every 0.5°C. The temperature was returned to 20°C at the end of each melt and the absorbance checked to ensure that solvent had not been lost by evaporation.

NMR samples

RNAs were dialysed extensively against NMR buffer (100 mM KCl, 50 mM NaCl, 4 mM Na cacodylate, 0.2 mM EDTA) in 1K MWCO tubing (Spectrum). RNA samples were concentrated to about 400 μl in a Centricon-3 concentrator (Amicon), and placed in a 5 mm NMR tube (Wilmad 528-PP). 20 μl of ^2H_2O and 0.5 μl of 2.5% dioxane were added to samples destined for exchangeable-proton spectroscopy as lock and chemical shift references. Samples intended for non-exchangeable proton spectroscopy were twice lyophilized and resuspended in 99.96% ^2H_2O, and then lyophilized and resuspended in 99.996% ^2H_2O plus 0.5 μl 2.5% dioxane in ^2H_2O.

NMR spectroscopy

Spectra were collected on the Yale 490 MHz spectrometer, a Bruker AM500, a GE Omega 500, a Varian Unity 500 and a Varian Unity+ 600. COSY, NOESY and TOCSY experiments were carried out on any of them as described (Szewczak *et al.*, 1993b). NOESY experiments

in H_2O suppressed water with jump-return spin echo and gradient echo sequences as described by Szewczak *et al*. (1993a). Natural-abundance ^{13}C-1H HSQC spectra were done on the Varian Unity+ 600. Phosphorus and phosphorus-proton experiments were executed on the AM500. ^{31}P-^{1}H COSY spectra were obtained as described (Sklenár *et al*. (1986) and ^{31}P-^{1}H heteroTOCSY and heteroTOCSY-NOESY spectra were taken as by Kellogg *et al*. (1992) and Kellogg (1992). The carrier was set at 4.7 p.p.m. for proton spectroscopy, −3.5 p.p.m. for ^{31}P, and 148 or 79 p.p.m. for ^{13}C, depending on the chemical shift range to be observed. ^{1}H chemical shifts were referenced to an internal dioxane standard (3.741 p.p.m.), ^{31}P chemical shifts to an external trimethyl phosphate standard (0 p.p.m.), and ^{13}C chemical shifts to an external sodium formate standard (26.1 p.p.m.). Data were processed on Silicon Graphics workstations using Felix (MSI).

Constraints for structure calculations

In regions judged to be *A*-form double helix, bases were constrained to pair by requiring that their hydrogen bond donor-acceptor distances be canonical, and by applying a pseudo-energy term that encouraged paired bases to be coplanar. *A*-form backbone configurations were enforced through the use of proton-proton distances derived from a model of an ideal *A*-form helix generated using Insight II (MSI), and by requiring that backbone and ribose torsion angles be within 15° of standard *A*-form values.

Distance constraints for the parts of the molecule that are not *A*-form were extracted from NOESY spectra collected at mixing times of 50, 100 and 300 ms. Correlations responsible for NOESY crosspeaks that were medium to strong at 50 ms were assigned a distance of 2.4 (±0.6) Å. Peaks which were absent or weak at 50 ms, but strong or medium at 100 ms, were assigned a distance of 3 (±1) Å, and peaks that were absent or weak at 50 and 100 ms, but detectable at 300 ms, were assigned a distance of 4 (±1) Å. Correlations involving 5′ or 5″ protons were assigned arbitrarily to one or the other, and the uncertainties in their distances increased by 1.8 Å, the distance between 5′ and 5″ protons.

H1′-H2′ coupling constants, $^{3}J_{H1'\text{-}H2'}$, were measured from COSY spectra as described by Kim & Prestegard, (1989). The fraction of C3′-*endo* character, $f_{C3'\text{-}endo}$, of each ribose ring was calculated as described (Altona, 1982; van den Hoogen, 1988).

Constraints for backbone dihedral angles α and ζ were inferred from ^{31}P chemical shifts (Gorenstein, 1984). The α and ζ angles of phosphorus atoms with *A*-like chemical shifts were constrained to *A*-form values ±30°. Both angles were left unconstrained for downfield-shifted phosphorus atoms. Since ^{31}P-^{1}H COSY spectra included no intense ^{31}P-H5′,H5″ crosspeaks, it was concluded that all βs were *trans*, and they were constrained to the *A*-form value ±30° (Varani & Tinoco, 1991). Since weak phosphorus-H4′ crosspeaks can be detected in ^{31}P-^{1}H COSY spectra only when β and γ are both *trans*, γ was constrained to the *trans*, *A*-form value ±30° for each nucleotide for which such a crosspeak was observed. Since ε is prevented from being *gauche*$^{+}$ (0° to 120°) by steric interactions, it was constrained to −120 (±120)° for all nucleotides (Varani & Tinoco, 1991).

Structure calculations

Structures were calculated with X-PLOR version 3 using the distance geometry/simulated annealing approach described in the X-PLOR manual (Brünger, 1992). The topology and parameter files used were derived (J. Rife unpublished results) from the heavy-atoms only topology/parameter set described recently (Parkinson *et al*., 1996). They are available at ftp://proton.chem.yale.edu/pub/rna-structure/.

Acknowledgments

D.C.S. thanks J. Kim for suggesting this project and the Howard Hughes Medical Institute for a predoctoral fellowship. This work was supported by a grant from the National Institutes of Health to P.B.M. (GM41651).

References

Altona, C. (1982). Conformational analysis of nucleic acids: determination of backbone geometry of single-helical RNA and DNA in aqueous solution. *J. Royal Neth. Chem. Soc.* **101**(12), 413–433.

Basavappa, R. & Sigler, P. B. (1991). The 3 Å crystal structure of yeast initiator tRNA: functional implications in initiator/elongator discrimination. *EMBO J.* **10**(10), 3105–3111.

Beckett, D. & Uhlenbeck, O. C. (1984). Enzymatic synthesis of oligoribonucleotides. In *Oligonucleotide Synthesis: A Practical Approach* (Gait, M. J., ed.), pp. 185–197, IRL Press, Oxford.

Brünger, A. T. (1992). *X-PLOR Version 3.1: A System For X-Ray Crystallography and NMR*, Yale University Press, New Haven.

Clore, G., Gronenborn, A., Piper, E., McLaughlin, L., Graeser, E. & Van Boom, J. (1984). The solution structure of a RNA pentadecamer comprising the anticodon loop and stem of yeast $tRNA^{Phe}$. A 500 MHz ^{1}H-N.M.R. study. *Biochem. J.* **221**(3), 737–751.

Dirheimer, G., Keith, G., Dumas, P. & Westhof, E. (1995). Primary, secondary and tertiary structures of tRNAs. In *tRNA: Structure, Biosynthesis and Function* (Söll, D. & RajBhandary, U., eds), pp. 93–126, American Society of Microbiology, Washington, DC.

Dube, S. K., Rudland, P. S., Clark, B. F. C. & Marcker, K. A. (1969). A structural requirement for codon-anticodon interaction on the ribosome. *C.S.H. Symp. Quant. Biol.* **34**, 161–166.

Fountain, M. A., Serra, M. J., Krugh, T. R. & Turner, D. H. (1996). Structural features of a six-nucleotide RNA hairpin loop found in ribosomal RNA. *Biochem.* **35**(21), 6539–6548.

Freier, S. M., Kierzek, R., Jaeger, J. A., Sugimoto, N., Caruthers, M., Neilson, T. & Turner, D. H. (1986). Improved free-energy parameters for predictions of RNA duplex stability. *Proc. Natl Acad. Sci. USA*, **83**, 9373–9377.

Gorenstein, D. & Goldfield, E. (1982). High-resolution phosphorus nuclear magnetic resonance spectroscopy of transfer ribonucleic acids: multiple conformations in the anticodon loop. *Biochemistry*, **21**(23), 5839–5849.

Gorenstein, D. G. (1984). Phosphorus-31 chemical shifts: principles and empirical observations. In *Phosphorus-31 NMR: Principles and Applications* (Gorenstein, D. G., ed.), pp. 7–36, Academic Press, Orlando, FL.

Guenther, R. H., Hardin, C. C., Sierzputowska-Gracz, H., Dao, V. & Agris, P. F. (1992). A magnesium-induced conformational transition in the loop of a DNA analog of the yeast $tRNA^{Phe}$ anticodon is dependent on RNA-like modifications of the bases of the stem. *Biochemistry,* **31**(45), 11004–11011.

Hartz, D., Binkley, J., Hollingsworth, T. & Gold, L. (1990). Domains of initiator tRNA and initiation codon crucial for initiator tRNA selection by *Escherichia coli* IF3. *Genes Dev.* **4**(10), 1790–1800.

Heus, H. A. & Pardi, A. (1991). Novel ^{1}H nuclear magnetic resonance assignment procedure for RNA duplexes. *J. Am. Chem. Soc.* **113**, 4360–4361.

Hingerty, B. E., Brown, R. S. & Jack, A. (1978). Further refinement of the structure of yeast $tRNA^{Phe}$. *J. Mol. Biol.* **124**, 523.

Holbrook, S. R., Sussman, J. L., Warrant, R. W. & Kim, S.-H. (1978). Crystal structure of yeast phenylalanine tRNA. II. Structural features and functional implications. *J. Mol. Biol.* **123**, 631.

Huang, S. G., Wang, Y. X. & Draper, D. E. (1996). Structure of a hexanucleotide RNA hairpin loop conserved in ribosomal RNAs. *J. Mol. Biol.* **258**(2), 308–321.

Jack, A., Ladner, J. E. & Klug, A. (1976). Crystallographic refinement of yeast phenylalanine tRNA at 2.5 Å resolution. *J. Mol. Biol.* **108**, 619–649.

Kellogg, G. W. (1992). Proton-detected hetero-TOCSY experiments with application in nucleic acids. *J. Magn. Reson.* **98**, 176–182.

Kellogg, G. W., Szewczak, A. A. F. & Moore, P. B. (1992). Two-dimensional hetero-TOCSY-NOESY: correlation of ^{31}P resonances with anomeric and aromatic ^{1}H resonances in RNA. *J. Am. Chem. Soc.* **114**, 2727–2728.

Kim, Y. & Prestegard, J. H. (1989). Measurement of vicinal couplings from cross peaks in COSY spectra. *J. Magn. Reson.* **84**, 9–13.

Kuchino, Y., Ihara, M., Yabusaki, Y. & Nishimura, S. (1982). Initiator tRNAs from archaebacteria show common unique sequence characteristics. *Nature,* **298**(5874), 684–685.

Labuda, D. & Porschke, D. (1982). Magnesium ion inner sphere complex in the anticodon loop of phenylalanine transfer ribonucleic acid. *Biochemistry,* **21**, 49–53.

Mandal, N., Mangroo, D., Dalluge, J. J., McCloskey, J. A. & RajBhandary, U. L. (1996). Role of the three consecutive G-C base pairs conserved in the anticodon stem of initiator tRNAs in initiation of protein synthesis in *Escherichia coli*. *RNA,* **2(5)**, 473–482.

Maniatis, T., Fritsch, E. F. & Sambrook, J. (1982). *Molecular Cloning: A Laboratory Manual,* Cold Spring Harbor Laboratory Press, Cold Spring Harbor, NY.

Meinnel, T., Mechulam, Y., Lazennec, C., Blanquet, S. & Fayat, G. (1993). Critical role of the acceptor stem of $tRNAs^{Met}$ in their aminoacylation by *Escherichia coli* methionyl-transfer RNA synthetase. *J. Mol. Biol.* **229**(1), 26–36.

Milligan, J. F., Groebe, D., Witherell, G. & Uhlenbeck, O. C. (1987). Oligoribonucleotide synthesis using T7 RNA polymerase and synthetic DNA templates. *Nucl. Acids Res.* **15**(21), 8783–8798.

Mirmira, S. R. & Tinoco, I. (1996a). NMR structure of a bacteriophage T4 RNA hairpin involved in translational repression. *Biochemistry,* **35**(24), 7664–7674.

Mirmira, S. R. & Tinoco, I. (1996b). A quadruple mutant T4 RNA hairpin with the same structure as the wild-type translational repressor. *Biochemistry,* **35**(24), 7675–7683.

Moore, P. B. (1995). Determination of RNA conformation by nuclear magnetic resonance. *Accts. Chem. Res.* **28**(6), 251–256.

Parkinson, G., Voitechovsky, J., Clowney, L., Brünger, A. T. & Berman, H. (1996). New parameters for the refinement of nucleic acid-containing structures. *Acta Crystallog. sect D,* **52**, 57–64.

Perona, J. J., Rould, M. A., Steitz, T. A., Risler, J.-L., Zelwer, C. & Brunie, S. (1991). Structural similarities in glutaminyl- and methionyl-tRNA synthetases suggest a common overall orientation of tRNA binding. *Proc. Natl Acad. Sci. USA,* **88**, 2903–2907.

Pley, H. W., Flaherty, K. M. & Mckay, D. B. (1994). Three-dimensional structure of a hammerhead ribozyme. *Nature,* **372**(6501), 68–74.

Rould, M., Perona, J., Soell, D. & Steitz, T. (1989). Structure of *E. coli* glutaminyl-tRNA synthetase complexed with $tRNA^{Gln}$ and ATP at 2.8 Å resolution. *Science,* **246**(4934), 1135–1142.

Saenger, W. (1983). *Principles of Nucleic Acid Structure,* Springer-Verlag, New York.

Salemink, P. J. M., Reijerse, E. J., Mollevanger, L. C. P. J. & Hilbers, C. W. (1981). Conformational changes of yeast $tRNA^{Phe}$ as monitored by ^{31}P NMR. *Eur. J. Biochem.* **115**, 635–641.

Schevitz, R. W., Podjarny, A. D., Krishnamachari, N., Hughes, J. J. & Sigler, P. B. (1979). Crystal structure of a eukaryotic initiator tRNA. *Nature,* **278**, 188–190.

Scott, W. G., Finch, J. T. & Klug, A. (1995). The crystal structure of an all-RNA hammerhead ribozyme: a proposed mechanism for RNA catalytic cleavage. *Cell,* **81**(7), 991–1002.

Seong, B. & RajBhandary, U. (1987). *Escherichia coli* formylmethionine tRNA: mutations of GGG:CCC sequence conserved in anticodon stem of initiator tRNAs affect initiation of protein synthesis and conformation of anticodon loop. *Proc. Natl Acad. Sci. USA,* **84**(2), 334–338.

Sklenár, V., Miyashiro, H., Zon, G., Miles, H. T. & Bax, A. (1986). Assignment of the ^{31}P and ^{1}H resonances in oligonucleotides by two-dimensional NMR spectroscopy. *FEBS Letters,* **208**(1), 94–98.

Sprinzl, M., Steegborn, C., Hubel, G. & Steinberg, S. (1996). Compilation of tRNA sequences and sequences of tRNA genes. *Nucl. Acids Res.* **24**(1), 68–72.

Striker, G., Labuda, D. & del Carmen Vega-Martin, M. (1989). The three conformations of the anticodon loop of yeast $tRNA^{Phe}$. *J. Biomolec. Struct. Dynam.* **7**(2), 235–256.

Szewczak, A. A., White, S. A., Gewirth, D. T. & Moore, P. B. (1990). On the use of T7 RNA polymerase transcripts for physical investigation. *Nucl. Acids Res.* **18**(14), 4139–4142.

Szewczak, A. A., Kellogg, G. W. & Moore, P. B. (1993a). Assignment of NH resonances in nucleic acids using natural abundance ^{15}N-^{1}H correlation spectroscopy with spin-echo and gradient pulses. *FEBS Letters,* **327(3)**, 261–264.

Szewczak, A. A., Moore, P. B., Chan, Y. L. & Wool, I. G. (1993b). The Conformation of the Sarcin/Ricin Loop

from 28S Ribosomal RNA. *Proc. Natl Acad. Sci. USA,* **90**(20), 9581–9585.
van den Hoogen, F. (1988). NMR studies concerning base-base interactions in oligonucleotides. Ph.D. thesis, Leiden.
Varani, G. & Tinoco, I. (1991). RNA structure and NMR spectroscopy. *Quart. Rev. Biophys.* **24**(4), 479–532.
Wakao, H., Romby, P., Westhof, E., Laalami, S., Grunberg-Manago, M., Ebel, J.-P., Ehresmann, C. & Ehresmann, B. (1989). The solution structure of the *Escherichia coli* initiator tRNA and its interactions with initiation factor 2 and the ribosomal 30S subunit. *J. Biol. Chem.* **264**(34), 20363–0371.
Westhof, E. & Sundaralingam, M. (1986). Restrained refinement of the monoclinic form of yeast phenylalanine transfer RNA: temperature factors and dynamics, coordinated waters, and base-pair propeller twist angles. *Biochemistry,* **25**(17), 4868–4878.
Westhof, E., Dumas, P. & Moras, D. (1988). Restrained refinement of two crystalline forms of yeast aspartic acid and phenylalanine transfer RNA crystals. *Acta Crystallog. sect. A,* **44**, 112.
Woo, N. H., Roe, B. A. & Rich, A. (1980). Three-dimensional structure of *Escherichia coli* initiator $tRNA_f^{Met}$. *Nature,* **286**, 346–351.
Wrede, P. & Rich, A. (1979). Stability of the unique anticodon loop conformation of E. coli $tRNA_f^{Met}$. *Nucl. Acids Res.* **7**(6), 1457–1467.
Wrede, P., Woo, N. H. & Rich, A. (1979). Initiator tRNAs have a unique anticodon loop conformation. *Proc. Natl Acad. Sci. USA,* **76**(7), 3289–3293.
Wüthrich, K. (1986). *NMR of Proteins and Nucleic Acids,* Wiley-Interscience, New York.
Zuker, M. (1989). On finding all suboptimal foldings of an RNA molecule. *Science,* **244**(4900), 48–52.

Edited by I. Tinoco

(Received 20 September 1996; received in revised form 2 December 1996; accepted 3 December 1996)